ACS OMEGA

http://pubs.acs.org/journal/acsodf

Article

Developing Structural First Principles for Alkylated Triphenylphosphonium-Based Ionic Liquids

Brianna O'Rourke,[⊥] Clare Lauderback,[⊥] Lara I. Teodoro,[⊥] Morgan Grimm, Matthias Zeller, Arsalan Mirjafari,* Gary L. Guillet, and Patrick C. Hillesheim*

Cite This: *ACS Omega* 2021, 6, 32285−32296

Read Online

ACCESS | Metrics & More | Article Recommendations | Supporting Information

ABSTRACT: While ionic liquids have proved to be versatile materials for a wide spectrum of applications, e.g., energy, materials, and medicine, several challenges remain concerning the rational design of novel materials. In light of this, a series of four triphenylphosphonium-based ionic liquids have been synthesized for the first time. These compounds exhibit high thermal stability with decomposition temperatures up to 450 °C. Their solid-state structures are characterized by single-crystal X-ray diffraction and the intermolecular interactions rigorously analyzed via Hirshfeld surface analysis. It was found that the unique geometries of the anions used in the study form distinct interactions with the cations. The interactions in the crystalline state are correlated with the thermal properties of the four ionic liquids to rationalize the melting points and phase transitions for each compound. The observed arrangements of the alkyl chains on the cations are investigated computationally to gain an understanding of how rotational freedom may impact the thermal properties of the compounds. By intention, each IL reported in this work offers a unique property profile and contributes to the ever-growing ionic liquid catalog.

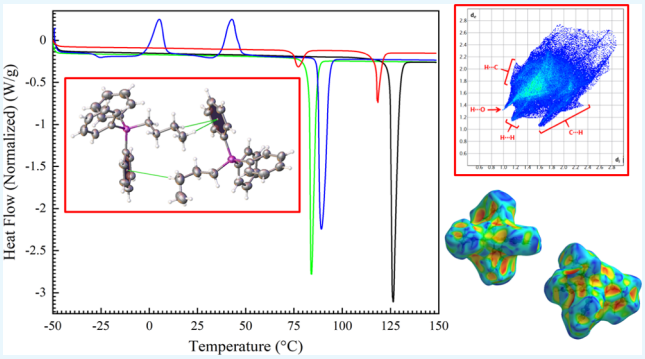

1. INTRODUCTION

Ionic liquids (ILs) are broadly defined as "a liquid comprised entirely of ions",[1] with the more commonly used definitions involving an ionic compound with a melting point below 100 °C.[2] With over 87 000 references in the literature to date, ILs have found widespread applications across a broad range of disciplines since the initial report of the modern air and moisture-stable ILs based on fluorinated anions in the 1990s.[3,4] Initially, $[PF_6]^-$ and $[BF_4]^-$ were used as common fluorinated anions to develop hydrophobic and moisture-stable ILs and these anions remain essential for IL development.[1,5] Perfluoroalkyl anions, such as bis(trifluoromethylsulfonyl)imide or $[TF_2N]^-$, and fluorinated alkyl phosphates have quickly become popular anions given their favorable properties.[6,7] Further, ILs based on imidazolium cations tend to be some of the most studied IL systems, boasting a combination of favorable physicochemical properties leading to low melting points,[8] lower viscosities,[9] and good electrical conductivity.[10] While 1-butyl-3-methylimidazolium bis(trifluoromethylsulfonyl)imide ($[C_4mim][TF_2N]$) remains one of the most studied and applied IL compounds to date, there remains a strong desire to explore other classes of ILs to tailor physical properties for a desired function.[11] The understanding of fundamental structure−property relationships of ILs has been developed in parallel with the exponential progress that has been made in exploiting ILs tailored for specific applications.[12] Crystallographic studies of ILs incorporating analysis of intermolecular forces are significant to understanding these structure−property relationships given the correlation of how short- and long-range orders affect the properties of ILs.[13−15]

Phosphonium ions are a readily available family of cations in the field of ILs, offering superior properties compared to nitrogen ion-based ILs for certain applications.[16,17] For example, phosphonium ILs were applied in the development of hydrophobic solvents for biomass processing while maintaining chemical stability due to the IL's lack of acidic hydrogens, as can be found in certain imidazolium cations.[18,19] Additionally, quaternary phosphonium ILs bearing long alkyl chains were found to have higher heat capacities when compared with imidazolium ILs.[20] Further, alkyl-bearing phosphonium ILs have been recently demonstrated to be useful in the fields of bioremediation as efficient media for CO_2

Received: September 21, 2021
Accepted: November 8, 2021
Published: November 16, 2021

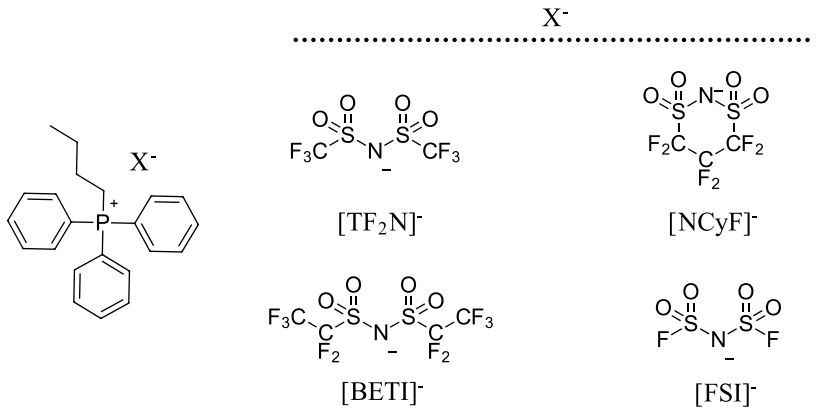

Figure 1. Depiction of the butyltriphenylphosphonium cation and four anions examined herein.

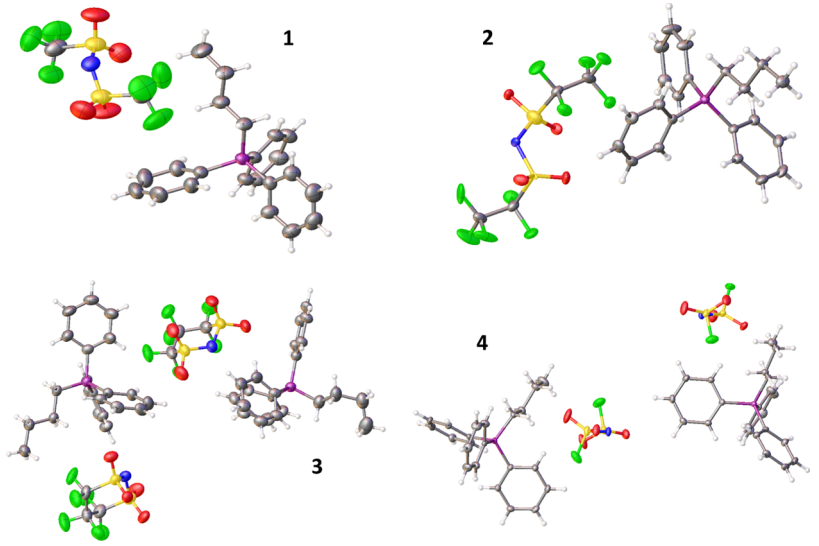

Figure 2. Asymmetric units of the crystal structures for compounds **1**−**4** shown with 50% probability ellipsoids. Disorder is omitted for clarity in **2** and **3**. Gray = carbon; blue = nitrogen; red = oxygen; green = fluorine; purple = phosphorous; yellow = sulfur; and white = hydrogen.

capture[21] and wastewater treatment.[22] Certain phosphonium ILs were also shown to be powerful pharmaceutical agents, facilitating the transport of biologically active compounds across cellular membranes.[23] In the 1970s, the initial details focusing on the development of phosphonium-based ILs were reported by the Parshall group,[24,25] employing stannate and germanate salts. In the 1980s, Knifton et al. reported the use of the molten salt $[P_{4444}][Br]$ as an ionic medium.[26−28] $[P_{4444}][Br]$ and $[P_{4444}][Cl]$, along with many other quaternary phosphonium salts, became commercially available on a large scale in 1990 when trialkylphosphine derivatives, in particular Bu_3P, were widely produced on a multiton scale by Cytec Industries Inc.[17,29] As such, quaternary alkyl-based phosphonium ILs are by far the preferred structural motif when it comes to the cation design given the necessity for asymmetry in the cationic moiety.[1,17] Perhaps due to the more symmetric structure of triphenylphosphine (TPP), few examples of ILs designed with this platform have been reported. However, TPP is an appealing starting material to develop ionic compounds due to its ready availability, low cost, and good chemical stability.

While IL chemists mostly rely on computational approaches to gain an enhanced understanding of intermolecular interactions within IL systems and the conformational states of each component of the salt, it is noteworthy that comparable methods taking advantage of crystallographic studies have been scarcely addressed.[30] Herein, we expand upon our previous works on TPP-derived ionic materials[31] by reporting the synthesis and characterization of four TPP-based ILs containing perfluoroalkyl anions (Figure 1). The thermal properties of the compounds are examined via thermogravimetric analysis (TGA) and dynamic scanning calorimetry (DSC) and the results of the thermal studies correlated to their crystal structures. Hirshfeld surface analysis of the cations is used to further evaluate intermolecular forces in the solid state to rationalize how changes in anion's geometry and composition affect the physicochemical properties of the ILs.[32−35] Additionally, computational studies on the conformations of the alkyl chain on the cation are used to rationalize the observed structures in the solid state. Of the four compounds reported, two have melting points below 100 °C with the remaining compounds melting slightly above 100 °C. Furthermore, the ILs have high thermal stabilities with decomposition temperatures up to 450 °C, making these ILs promising candidates for higher-temperature applications. Moreover, the highly crystalline nature of the alkylated-TPP cations provides an excellent opportunity to examine the relatively unstudied solid-state structures of bis-

https://doi.org/10.1021/acsomega.1c05241
ACS Omega 2021, 6, 32285−32296

(pentafluoroethanesulfonyl)imide ([BETI]$^-$), 1,1,2,2,3,3-hexafluoropropane-1,3-disulfonimide ([NCyF]$^-$), and bis(fluorosulfonyl)imide ([FSI]$^-$) anions. These three fluorinated anions have shown promise in many IL applications, yet remain out of favor when compared with the structurally related [TF_2N]$^-$ anion.

2. RESULTS AND DISCUSSION

2.1. Structural Analysis. The asymmetric units of all four structures are shown in Figure 2. Both compounds **1** and **3** crystallize in an orthorhombic crystal system ($Pna2_1$ and $Pca2_1$ respectively), compound **2** is triclinic in the $P\bar{1}$ space group, and compound **4** is monoclinic with the $P2_1/n$ space group. Both **1** and **2** have a single cation−anion pair in the asymmetric unit, while **3** and **4** have two sets of distinct cations and anions. Additionally, **3** has a rotationally disordered cation wherein one entire cation moiety is rotated in a two-part disordered system. For the purposes of discussion regarding **3** and its surfaces and interactions, the major portion of the disorder is used for analysis unless specifically noted.

In general, all cations show comparable structures with two of the phenyl rings (labeled B and C) being canted with respect to each other (plane angles ∼77°). The third ring (labeled A) is also rotated out of the plane (Figure 3). This

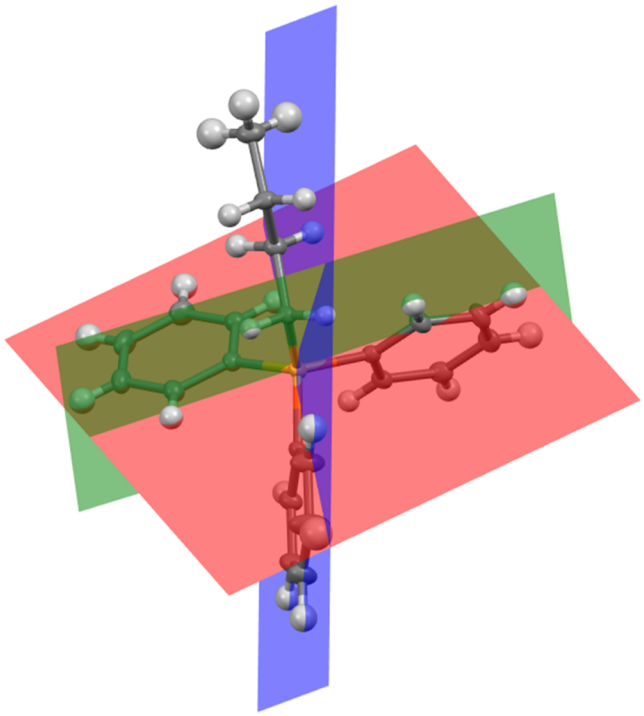

Figure 3. Depiction of the planes of each aryl ring of the cation from **2** showing the alignment of the planes with respect to each other and the central alkyl chain.

structural arrangement is seen in nearly all quaternary triphenylphosphonium examined in the CSD.[49] It has been well established that symmetry of the cation plays an important role in the melting points of ILs,[1,13,50] thus the observed arrangement of the cations does impart a certain asymmetry around the cation perhaps leading to the lower than expected melting points for the compounds examined herein.

One notable difference in the cation structure arises from the cation in **3**. The butyl chain of one of the two crystallographically independent cations has an anti-conformation, similar to **1**, **2**, and **4**. The second cation, on the other hand, shows a more complicated behavior. It is disordered, with both gauche- as well as anti-conformations. The major moiety butyl chain exists in a gauche-conformation with a C23−C24−C25−C26 torsion angle of 57.2°. This conformation of the alkyl chain on the phosphorous atom also exists in all of the reported halide precursor structures, that is butyltriphenylphosphonium chloride,[51] bromide,[52] and the iodide,[53] and is observed in several other structures. To gain a better understanding of this structural feature, conformational analysis was performed on the butyl chain of the cation (Figure 4). The relative energies of the gauche- and anti-conformations

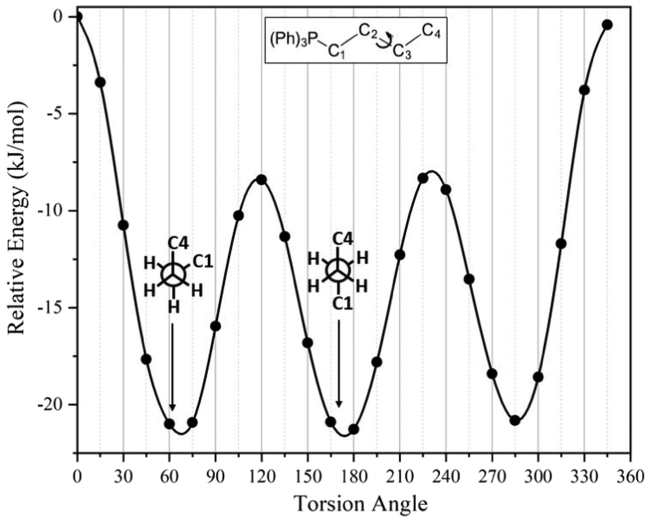

Figure 4. Graph showing the relative energies of the differing conformers of the butyl chain on the cation.

are very close with only a difference of approximately 0.3 kJ/mol between the two isomers. This small difference in energy explains the prevalence of the gauche-conformation in the solid state. Further, this difference in energy may help explain the relatively low melting points of the salts by allowing multiple orientations of the butyl chain in the solid state, as evidenced by the disorder observed in the crystal structure. This is likely to disrupt or weaken the lattice energy of the solid state, thus lowering the melting points of this class of compounds.[54] Further, these multiple orientations explain, in part, the observed thermal properties of **1** with the multiple solid−solid transitions seen in the DSC (vide infra).

To further our understanding of the compounds, Hirshfeld surface analysis of the cations was performed.[32−35] The surfaces and fingerprint plots of the cations are shown in Figure 5. The relative percentage of interactions arising from individual atoms is summarized in the Supporting Information. Examining the fingerprint plots, the four structures share several characteristic features, as annotated in the images. For instance, **1** and **3** have similar fingerprint plots with a distinct two-winged feature arising from π-interactions in the solid state. Additionally, all of the plots display hydrogen interactions, which are manifested as the sharp spikes labeled in the plots. The individual spikes, however, are comprised of unique hydrogen interactions for each compound. Finally, all four of the compounds exhibit a region of increased interactions represented by the green portion of the plots, which mostly coincide with the uppermost spikes in each

https://doi.org/10.1021/acsomega.1c05241
ACS Omega 2021, 6, 32285−32296

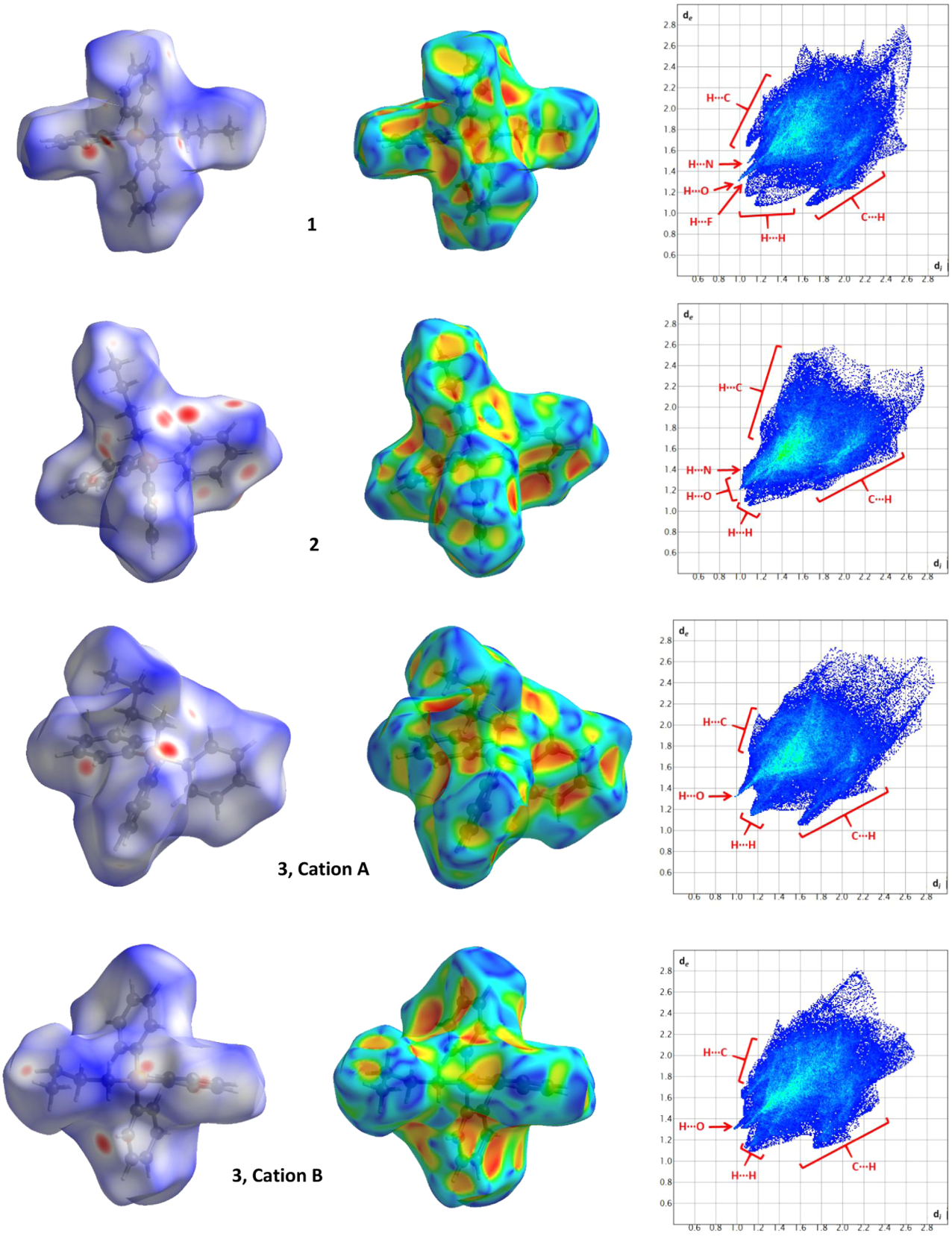

Figure 5. continued

https://doi.org/10.1021/acsomega.1c05241
ACS Omega 2021, 6, 32285−32296

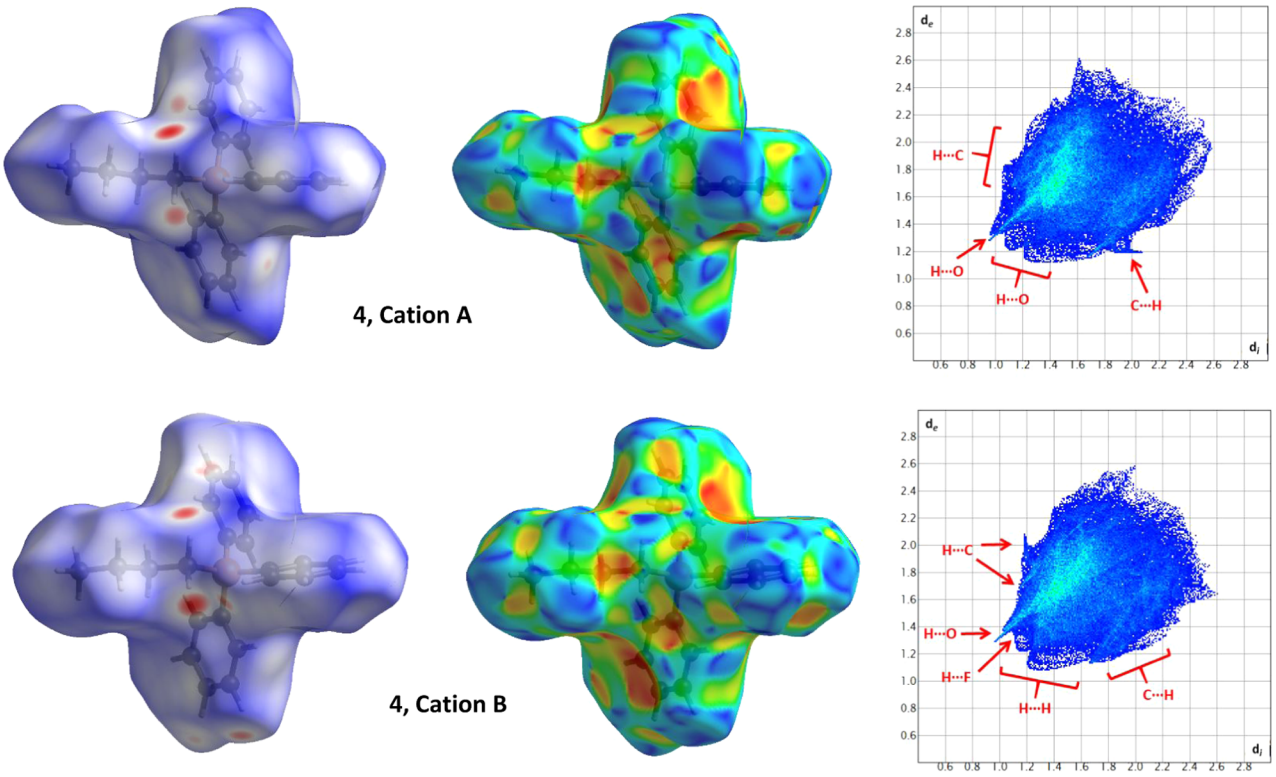

Figure 5. Surfaces and fingerprint plots for cations in the crystal structures. (Left) Hirshfeld surface mapped with d_{norm}, (middle) Hirshfeld surface mapped with the shape index (right), and fingerprint plots of the cations.

cation and are overlapping regions of H···O, H···F, and H···H interactions. Despite the similarities in both structure and composition of the compounds, all four of the molecules present distinctive physical properties, which can be attributed to the geometry of the anions and their impact on cation−cation interactions.

With regards to the hydrogen bonding, **1** shows H···X interactions with all three electronegative moieties (X = N, O, F). Three distinct spikes are seen corresponding to these interactions, which are labeled in Figure 5. The shortest H···O interactions arise from contacts between the aryl hydrogens closest to the cationic phosphorous (ortho hydrogens) and the sulfonyl oxygen atoms at distances of approximately 2.4 Å. Longer interactions are seen with the alkyl hydrogens on carbons C1 and C2 ($d \approx 2.8-3.8$ Å); however, these interactions appear far less significant as cation−anion interactions, when compared to the aryl hydrogens, based on their increased distances. As has been observed with other $[TF_2N]^-$ containing IL structures, the S═O···H interactions tend to be the shortest cation−anion interactions.[5,55,56]

As with the H···O interactions, the H···F interactions are shortest with the ortho hydrogens at distances of approximately 2.5 Å. The fluorine atoms appear to interact more readily with the alkyl hydrogens with a significant portion of the surface surrounding the alkyl hydrogens displaying some form of interaction with any number of fluorine atoms. Finally, the central imide nitrogen on the $[TF_2N]^-$ makes a notably short H···N interaction with an aryl hydrogen (C6C−H) at a C−H···N distance of 2.72 Å.

The wings on the periphery of the fingerprint plot correspond to reciprocal H···C|C···H π interactions. These interactions are seen between both the aryl and alkyl hydrogens on the π-system of the three rings. Interactions are seen arising from all three of the rings on the cation giving rise to a unique stacking of the cations, as seen in Figure 6.

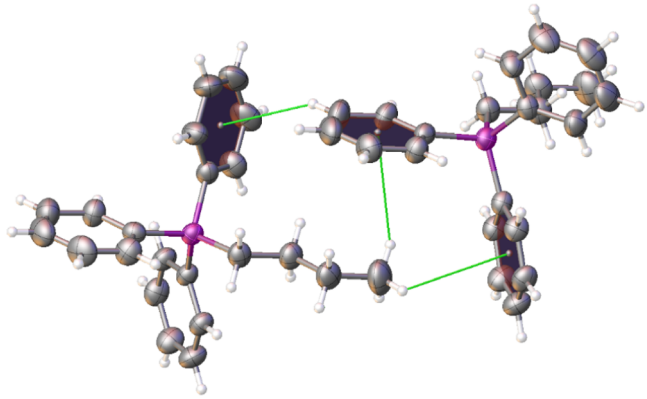

Figure 6. Depiction of cation···cation interactions observed in **1**. Green lines are used to visualize interactions with the π systems of the rings (shaded).

While less prominent, in terms of percentage, F and O···π interactions are also seen in the structure. These interactions, however, do not manifest into a salient plot feature and are buried in the bulk of the plot at approximately $d_i = 1.8$, $d_e = 1.5$.

While compound **2** shows a similar set of H···X interactions as the other compounds given the unique geometry and conformers available to the $[BETI]^-$ anion,[57−59] distinct interactions are observed in the fingerprint plots. For example, with regards to H···O interactions, the $[BETI]^-$ anion in **2** interacts mostly with aryl hydrogens, in a manner that is observed in all of the compounds discussed herein. However,

https://doi.org/10.1021/acsomega.1c05241
ACS Omega 2021, 6, 32285−32296

the anion is seen to interact with all hydrogens on the aryl rings as opposed to just the ortho hydrogens, as is seen in **1**. Further, only C1 and C2 on the alkyl chain interact with the sulfonyl oxygens. The hydrogens participating in the H···O interactions are predominantly on the face of the molecule aligned with the alkyl chain, likely due to the increased anion size. This is distinct from the interactions observed with $[TF_2N]^-$, wherein the anion in **1** is seen to interact closest with the hydrogens on the opposite face of the alkyl chain, in the cavity formed by the three aryl rings on the opposite face of the alkyl chain. These interactions on **2** are seen as the bright red spots on the surface, as seen in Figure 5. The H···F interactions comprise the majority of the interactions of the alkyl chain hydrogens, as with all of the compounds. Finally, weaker H···N interactions are seen; however, these interactions are difficult to quantify as the nitrogen in the anion is disordered around a crystallographic inversion center.

Compound **2** shows no defined H···π interactions, as noted by the absence of the wing feature in the fingerprint plots. While there is a percentage of H···C interactions (see the Supporting Information), the arrangement of the cations in the solid state is such that the hydrogens do not interact with the centers of the π systems of the aryl rings (see Figure 7). These

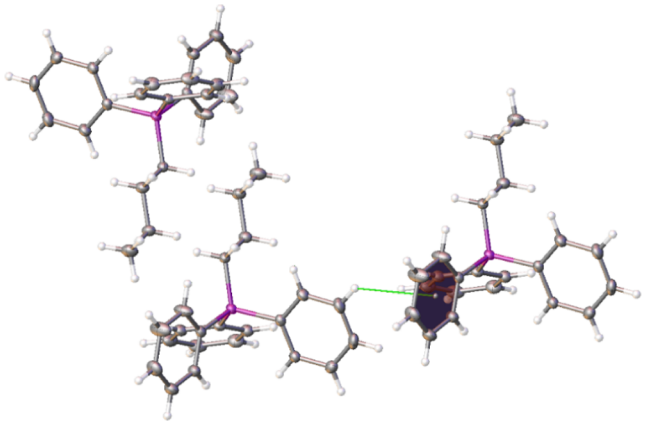

Figure 7. Depiction of cation···cation interactions observed in **2**. Green lines are used to visualize interactions with the π systems of the rings (shaded).

shifted H···π interactions are likely one reason for the lower melting point of **2** as compared to the other compounds. However, **2** does show the highest percentage of C···F interactions, indicating significant interactions between the π system and the fluorine atoms of the anion. In part, this increased percentage of interactions is rationalized by the $[BETI]^-$ anion having the highest percent composition of fluorine atoms. The perfluoro ethyl moiety on the anion sits in a pocket between rings B and C on the cation, forming a bridge between the two through C···F···C interactions at distances of approximately 3.0 Å.

Compound **3** has two cations in the asymmetric unit with each showing a unique fingerprint due, in part, to the gauche-conformation of the alkyl chain in one of the cations (the minor moiety anti-conformation of the second cation was not considered in the Hirshfeld surface analyses). As anticipated, related structural features are seen in **3** similar to those discussed in the other compounds such as a blunted H···H interaction peak, hydrogen bonding spikes, and wings indicating π interactions. As with all of the compounds, the sulfonyl oxygens make the shortest H-bonding contacts with the ortho hydrogens. Similar to described for compound **2**, the anions in **3** have the shortest interactions with the ortho hydrogens, which are oriented toward the alkyl chain in both cationic moieties of the asymmetric unit.

3 exhibits typical H···F interactions with both the alkyl and aryl hydrogens, but it has a lower percentage of interactions when contrasted with **1** and **2**. The arrangement of the alkyl chain clearly impacts the anion−cation interactions as is noted with the difference in H···F interactions between the two cationic moieties. Further, the H···N interactions are the highest in **3** compared with the other compounds. This increased interaction from the imide nitrogen is expected, however, as the nitrogen moiety on the anion has a larger exposed surface area when compared to $[TF_2N]^-$ or $[BETI]^-$.[60]

Both cations in **3** display H···π interactions, as seen by the presence of the wing features on the plots (d_i = 1.2, d_e = 1.7). Cation **3A** has close H···C|C···H interactions with **3B** through aryl hydrogens, which manifests as the indicated wings in each plot (see Figure 8). The two unique wings represent

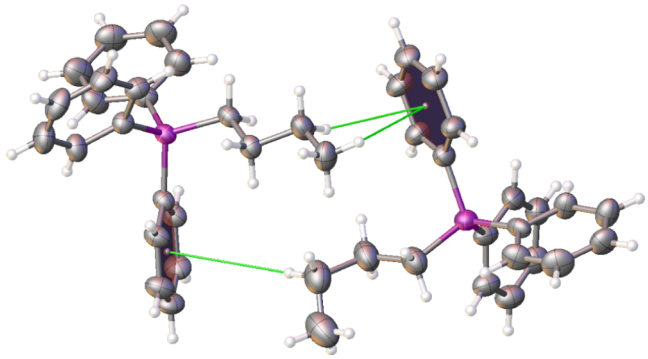

Figure 8. Depiction of cation···cation interactions observed in **3**. Green lines are used to visualize interactions with the π systems of the rings (shaded). Disorder omitted for clarity.

interactions with the alkyl chain hydrogens at d_i = 1.1, d_e = 1.6 and with aryl hydrogens at d_i = 1.5, d_e = 1.1. While the two wings do have overlap with respect to reciprocal interactions, the unique shape of the wings is due to the type of hydrogen atoms involved in the interactions.

The structure of **4** contains two ion pairs in the asymmetric unit and both $[FSI]^-$ anions are found in the trans, or C_2, conformation.[61] Similar to the discussion with the other compounds, both cations in **4** exhibit hydrogen bonding and π interactions. As seen in **1**, the anions in **4** show interactions with the pocket formed by the three phenyl rings on the opposite face from the alkyl chain in the cation. The ortho hydrogens are the shortest interactions with the sulfonyl oxygens (d_i = 0.7, d_e = 1.3) for both cations. Cation **4B** shows the highest interaction between the imide nitrogen and the π system of a benzene ring, albeit to a small extent. While unique for this set of compounds, the N···π interactions have been observed in previous structures.[62] Likely, the decreased sterics of the smaller $[FSI]^-$ anion allows for these interactions to form.

As is seen by the unique wing shape in **4**, the π interactions are unique. Specifically, the H···C|C···H interactions in **4** are found to align the cations in a manner wherein the alkyl groups are oriented in the same direction through aryl H···C

https://doi.org/10.1021/acsomega.1c05241
ACS Omega 2021, 6, 32285−32296

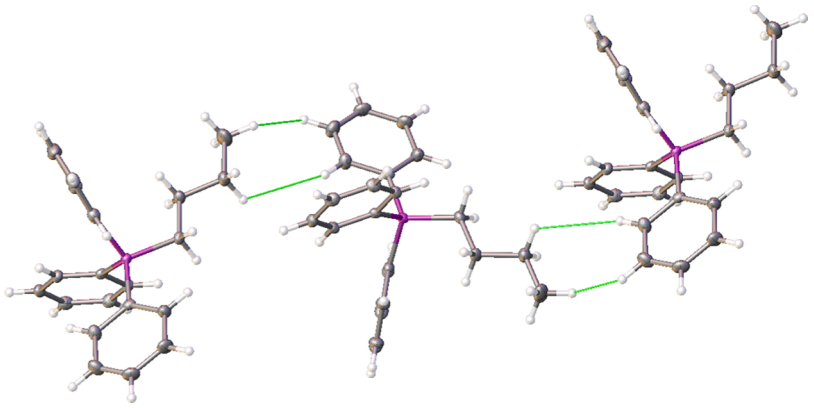

Figure 9. Depiction of cation···cation interactions observed in **4**. Green lines are used to visualize interactions.

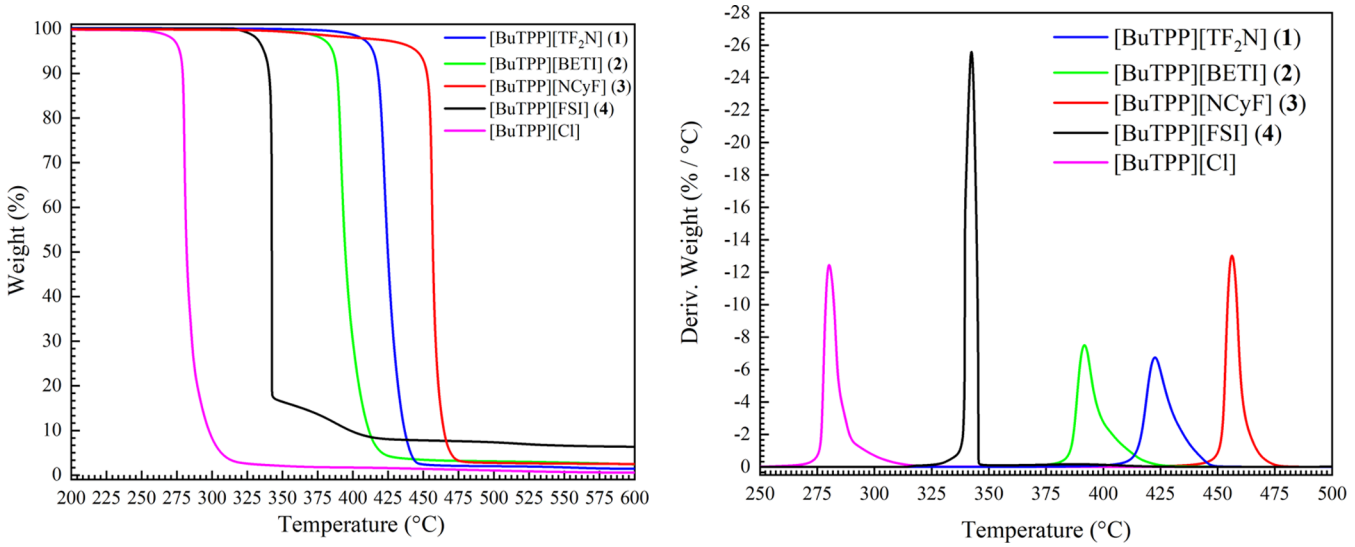

Figure 10. TGA (left) and DTG (right) traces for **1**−**4** compared with the starting material [BuTPP][Cl].

interactions (Figure 9). This alignment of the alkyl groups then allows the C4−H···π alkyl interactions to direct enhanced long-range ordering.

2.2. Thermal Properties. The thermal properties of the four compounds were evaluated using TGA and DSC, and the respective traces are shown in Figures 10 and 11 with a summary of thermal properties in Table 1. For the thermal stability studies, the compounds are contrasted to the starting material, namely, butyltriphenylphosphonium chloride, [BuTPP][Cl]. Compounds **1**−**3** show nearly identical decomposition profiles, with a single large step occurring and no residual material formation. **4** shows a two-step decomposition wherein a large initial step at 325 °C is followed by a subsequent plateau with the formation of a residual material, seen as the residual weight in the TGA trace. Given the cation is constant, the large decomposition step seen in all compounds must correspond to the degradation of the cation given the profile of the step. In line with reported trends, the $[NCyF]^-$ bearing compound exhibits the highest $T_{decomp.}$, followed by $[TF_2N]^-$ and then $[BETI]^-$.[8,58] All fluorine-bearing anion compounds showed significantly higher thermal stabilities than the chloride starting material, indicating that TPP-based ILs should follow the established trends for ILs.[8,20,63,64] While $T_{decomp.}$ is a useful screening metric for establishing thermophysical parameters of ILs, long-term thermal stability is a more useful property for applicability of ILs for specific tasks wherein extended elevated temperatures would be required.[63]

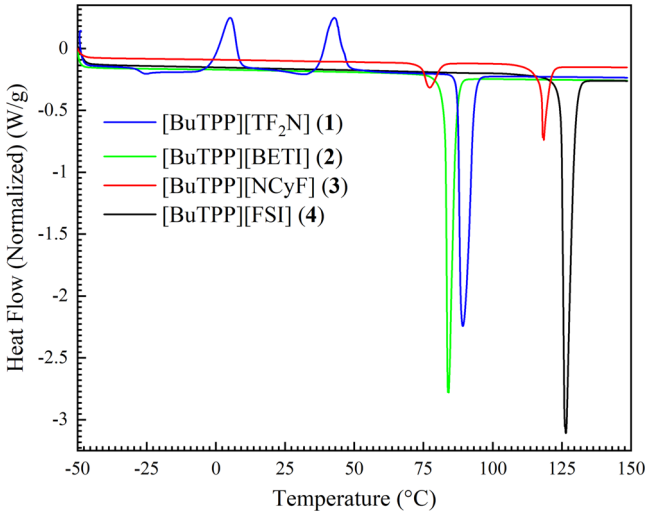

Figure 11. DSC traces from the first heating cycle for the ILs **1**−**4**.

The phase transitions for **2** are rather simple, showing a sharp melting point followed by glass transitions upon repeated

https://doi.org/10.1021/acsomega.1c05241
ACS Omega 2021, 6, 32285−32296

Table 1. Compiled Thermophysical Properties of Compounds 1−4

compound	$T_{decomp.}$ [a]	T_m [b]	ΔH_m [c]	T_g	T_{cc} [d]	
1	422.61	89.32	49.09	−27.32	8.36	45.50
2	391.77	85.20	43.49	−25.44		
3	456.24	118.50	11.86			
4	342.40	126.44	60.12			

[a]Decomposition temperature in °C taken from the maximum rate of the DTG. [b]Melting point (°C). [c]Enthalpy of melting (J/g). [d]Temperature of cold crystallization (°C).

cycles. As seen in Table 1, the melting point for **2** (85.20 °C) is the lowest of the compounds, followed by **1** (89.32 °C) and with **3** and **4** melting at 118.50 °C and 126.40 °C, respectively. As discussed previously, the absence of specific π interactions in **2** could rationally account for this observation. **1** has the lowest glass transition, followed closely by **2**. No glass transitions are observed for **4**; however **4**, was the only compound to show a crystallization peak during cooling. It should be noted that **1** has additional exothermic transitions, with two solid−solid transitions appearing at 4.6 and 43.2 °C. We speculate that these peaks correspond to transitions to a stable or metastable crystalline[65] form with different alkyl chain conformations present (vide supra), the existence of a polymorph wherein a cation is oriented in a different manner similar to that seen in compound **3**, or a form wherein the cis form of the $[TF_2N]^-$ anion is present.[66,67] Compound **3** also exhibits an endothermic phase transformation at 77 °C before melting at 118 °C. While the exact reason for this transition is not known, previous structures with this anion have indicated the presence of unique conformers.[60] Neither the phase transformation nor the larger endothermic melting peaks are observed in subsequent heating/cooling cycles.

The enthalpy values for melting (ΔH_m), however, show a complex relationship between intermolecular interactions and the thermal behavior of ILs.[11] There is no overt correlation between interactions and enthalpy values. For example, both **1** and **2** have similar melting points and enthalpy values yet vary significantly in the percentage and nature of the crystalline interactions discussed. Compound **3** has a distinctly lower enthalpy (ΔH_m = 11.8 J/g) when compared to the other three compounds. This is not unusual, however, as the $[NCyF]^-$ anion has shown smaller enthalpies in our previous studies despite having higher melting points.[60] As data is continued to be collected on these and related samples, we hope that distinct trends will start manifest allowing for the prediction of properties based on crystallographic and experimental evidence.

3. CONCLUSIONS

Four new phosphonium-based ILs have been studied in the solid state using single-crystal X-ray diffraction. The reported crystallographic analysis of these ILs provides direct insight into the spatial relationships between the phosphonium cation and perflourinated anions, providing the foundation for a fundamental understanding of their structure−property correlations. Several key interactions are observed when examining the Hirshfeld surfaces of these compounds. For example, aryl hydrogens are found to participate more readily in hydrogen interactions with the sulfonyl oxygens on the anions. The alkyl hydrogens, on the other hand, are found interacting predominantly with the fluorine moieties on the anions. However, both sets of hydrogens are observed to participate in H···π interactions, though the geometry of the anion appears to dictate the extent and nature of these interactions.

The aryl rings on the cation appear in similar geometric arrangements in the structures, with the preferred orientation showing ring A canted with respect to B and C. As seen in previously reported structures, and again observed herein, the alkyl chain on the cation readily adopts a gauche-conformation, though calculations indicate a slight energetic preference for the staggered anti-arrangement. The canted rings along with the accessible conformations of the alkyl chain are proposed as reasons for the lower than anticipated melting points of **1** and **2**, despite the ion pairs having high molecular weights.

The thermal properties of the four compounds are promising, with **1** melting at ∼90 °C and remaining a liquid up to 420 °C, displaying a sizable liquid range for the compound. All four compounds display high decomposition temperatures, in line with other reported phosphonium-based ILs. Overall, two of the compounds are classical ILs with T_m less than 100 °C, and the remaining two compounds are melting around 120 °C. The long-term thermal stabilities of the compounds are currently being evaluated to assess the utility of these new ILs.

This class of ILs shows unique interactions and properties controlled, ostensibly, by the choice of the anion. This would make them attractive for separations applications, especially given their high thermal stability. Further, we anticipate their use as high-temperature conductive materials[68] or solvents.[69] Finally, aside from their thermal properties, these ILs have a highly crystalline nature, lending to their potential use as crystallization media.[70] Despite intense interest in P(V) organophosphorus chemistry in the fields of biochemistry and organic synthesis,[71] the potential of ionizable P(V)-based compounds has not been fully embraced. The exquisite chemical stability and crystallinity of these phosphonium salts could make it a go-to strategy for those interested in synthesizing and studying molecules of life (oligonucleotides) and to those interested in basic organic transformations.[72]

4. MATERIALS AND METHODS

4.1. Chemicals. 1-Butyltriphenylphosphonium chloride was purchased from Fisher Scientific or synthesized following established literature procedures.[36] Lithium bis-(trifluoromethane)sulfonimide ($LiTF_2N$) was purchased from ChemImpex. Lithium 1,1,2,2,3,3-hexafluoropropane-1,3-disulfonimide (LiNCyF) was purchased from TCI Chemicals. Lithium bis(pentafluoroethanesulfonyl)imide (LiBETI) was generously donated by Prof. Jim Davis' Laboratory at the University of South Alabama. All reagents were used as received without further purification.

4.2. Spectroscopy. ^1H, ^{13}C, and ^{19}F NMR spectroscopies were performed on a JEOL 400 MHz NMR. Deuterated NMR solvents were purchased from Cambridge Isotope Labs. Chemical shifts were referenced to the residual solvent peaks in the NMR spectra. Complete NMR spectra are provided in the Supporting Information.

4.3. Thermal Properties. Melting points, glass transitions, and crystallization temperatures were measured using a TA instruments Q200 differential scanning calorimeter (DSC). Each sample was placed in an aluminum pan and cycled three consecutive times from −50 to 150 °C at a heating and cooling rate of 10 °C/min with nitrogen as a purge gas. A 3-min

https://doi.org/10.1021/acsomega.1c05241
ACS Omega 2021, 6, 32285−32296

isothermal step was included at the minimum and maximum temperatures of each cycle. Enthalpy values for the phase transitions were calculated using the TRIOS software from TA Instruments.

Decomposition temperatures were measured on a TA instruments Q500 thermogravimetric analyzer (TGA) using the default dynamic settings for the system and using a platinum pan under an N_2 atmosphere. The differential thermogravimetric curves (DTG) were obtained from the experimental TGA data and visualized with the OriginPro software. Decomposition temperatures were obtained using the maximum thermal decomposition rate of each DTG curve.

With respect to the discussion of melting points and the reported thermal data (see Table 1), these were acquired from individual DSC runs. Compounds **1** and **4** display consistent melting points across all three cycles. Compounds **2** and **3**, however, simply show one melting transition on the first heating cycle. The complete listing of all melting points from the individual runs is provided in the Supporting Information.

4.4. Single-Crystal Diffraction. Single crystals for compound **1** were coated in Cargille Type A immersion oil and transferred to the goniometer of a Rigaku XtalLAB Mini diffractometer with Mo Kα wavelength (λ = 0.70926 Å) and a CCD area detector. Examination and data collection were performed at 170 K.

Single crystals of compound **2** and **4** were coated with Parabar 10312 oil and transferred to the goniometer of a Bruker D8 Quest Eco diffractometer with Mo Kα wavelength (λ = 0.71073 Å) and a Photon II area detector. Examination and data collection were performed at 100 K.

Single crystals of compound **3** were coated with a trace of Fomblin oil and were transferred to the goniometer of a Bruker Quest diffractometer with kappa geometry, a Cu Kα wavelength (λ = 1.54178 Å) I-μ-S microsource X-ray tube, laterally graded multilayer (Goebel) mirror for monochromatization, and a Photon II area detector. Examination and data collection were performed at 150 K.

For compound **1**, data were collected, reflections were indexed and processed, and the files were scaled and corrected for absorption using CrysAlis PRO.[37] For compounds **2**−**4**, data were collected, reflections were indexed and processed, and the files were scaled and corrected for absorption using APEX3[38] and SADABS.[39] For all compounds, the space groups were assigned using XPREP within the SHELXTL suite of programs;[40,41] the structures were solved by direct methods using ShelXS or ShelXT[42] and refined by full-matrix least-squares against F^2 with all reflections using Shelxl2018[43] using the graphical interfaces Shelxle[44] and/or Olex2.[45] H atoms were positioned geometrically and constrained to ride on their parent atoms. C−H bond distances were constrained to 0.95 Å for aromatic and alkene C−H moieties and to 0.99 and 0.98 Å for aliphatic CH_2 and CH_3 moieties, respectively. Methyl H atoms were allowed to rotate, but not to tip, to best fit the experimental electron density. $U_{iso}(H)$ values were set to a multiple of $U_{eq}(C)$ with 1.5 for CH_3 and 1.2 for C−H and CH_2 units.

In the structure of **2**, two crystallographically independent anions are both disordered across inversion centers. The disordered moieties were restrained to have similar geometries. Atoms C11A and C13A, C12A and C14A, C11B and C13B, C12B and C14B, and S1A and S2A were each constrained to have identical ADPs. A global rigid bond restraint (RIGU) was applied. In the structure of **3**, one of the cations is disordered by swapping the butyl position with one of the phenyl groups. The disorder was extended to the entire cation. Both disordered moieties were restrained to have similar geometries as the other not disordered cation. U^{ij} components of ADPs for disordered atoms closer to each other than 2.0 Å were restrained to be similar. Subject to these conditions, the occupancy ratio refined to 0.655(5) to 0.345(5).

Complete crystallographic data, in the CIF format, have been deposited with the Cambridge Crystallographic Data Centre. CCDC 2108559−2108562 contains the supplementary crystallographic data for this paper. These data can be obtained free of charge from The Cambridge Crystallographic Data Centre via www.ccdc.cam.ac.uk/data_request/cif.

Hirshfeld surfaces, images, and fingerprint plots were calculated and produced using CrystalExplorer17.[46,47] Images and analysis of the structures were accomplished using Olex2. Hirshfeld surface analysis considers a "whole molecule" approach to examining interactions in a crystalline solid.[32] In brief, surrounding a crystallographic moiety with a weighted surface allows for analysis of the interactions via the overlap of surfaces. These interactions are typically reported as d_i and d_e values, wherein the *i* and *e* simply refer to interatomic distances to the inside or exterior of the surface. The Hirshfeld surface can be mapped with several functions such as d_{norm}, which is a visualization of the normalized distances of atoms, allowing for facile interpretations of interactions, which are displayed as variable colors (blue = long interactions, white = near van der Waals radius, red = short).[47] The surface analysis can be deconstructed into 2D fingerprint plots allowing for visualization of interactions via salient patterns such as hydrogen bonding (spikes) and π interactions (wings).[33] Interactions with π systems are denoted by interactions with "C" following the standard results of the surface analysis.[33]

4.5. Computational Studies. All computations and resultant data were obtained using the Spartan software suite (Spartan'18, Wavefunction, Inc., Irvine, CA). The initial geometry of the major portion of the disordered cation from compound **3** was loaded into the software and optimized employing the ωB97X-D functional[48] with a 6-311++G(d,p) basis set. Vibrational frequencies were checked for imaginary values to ensure that the resultant structures were at a minimum. The torsion angle of atoms C1−C2−C3−C4 was scanned from 0 to 360° in 15° steps and the relative energies of the conformers were used for discussion.

5. EXPERIMENTAL SECTION

5.1. Formation of the Ionic Liquid Compounds. *5.1.1. [BuTPP][TF_2N] (1).* Butyltriphenylphosphonium chloride (0.20 g, 0.56 mmol) was dissolved in the minimum amount of water to completely dissolve the salt. Lithium bis-(trifluoromethane)sulfonimide (0.16 g, 0.67 mmol) was added to the solution at room temperature and a white precipitant formed immediately. The mixture was stirred at room temperature for 2 h, filtered, and washed with cold water (3 × 10 mL). The white solid was dried under vacuum overnight at 50 °C (0.28 g, 84% isolated yield).

^{1}H NMR (400 MHz; $CDCl_3$) δ 7.83−7.62 (m, 15H), 3.12 (d, J = 14.2 Hz, 2H), 1.60 (d, J = 28.0 Hz, 4H), 0.92 (d, J = 6.4 Hz, 3H).

^{13}C NMR (101 MHz; $CDCl_3$) δ 135.4, 133.3, 130.7, 124.8−115.2, 118.4−117.5, 24.4, 23.7, 22.2, 13.4.

^{19}F NMR (376 MHz; $CDCl_3$) δ −78.6 (s).

https://doi.org/10.1021/acsomega.1c05241
ACS Omega 2021, 6, 32285−32296

*5.1.2. [BuTPP][BETI] (**2**).* Compound **2** was synthesized in the same manner as **1** using LiBETI as the anion source (0.36 g, 92% yield).

^{1}H NMR (400 MHz; $CDCl_3$) δ 7.81 (td, J = 7.3, 1.7 Hz, 3H), 7.72−7.61 (m, 12H), 3.16−3.09 (m, 2H), 1.62−1.53 (m, 4H), 0.90 (t, J = 6.9 Hz, 3H).

^{13}C NMR (101 MHz; $CDCl_3$) δ 135.4, 133.3, 130.7, 117.9, 122.8−108.2, 24.4, 23.6, 22.2, 13.4.

^{19}F NMR (376 MHz; $CDCl_3$) δ −78.8, −117.0.

*5.1.3. [BuTPP][NCyF] (**3**).* Compound **3** was synthesized in the same manner as **1** using LiNCyF as the anion source (0.31 g, 90% yield).

^{1}H NMR (400 MHz; $CDCl_3$) δ 7.83−7.78 (m, 3H), 7.73−7.62 (m, 12H), 3.21−3.14 (m, 2H), 1.63−1.55 (m, 4H), 0.91 (t, J = 7.0 Hz, 3H).

^{13}C NMR (101 MHz; $CDCl_3$) δ 135.4, 133.4, 130.7, 117.9, 116.0, 113.1, 110.1−109.7, 24.4, 23.7, 22.3, 13.4.

^{19}F NMR (376 MHz; $CDCl_3$) δ −119.3, −126.0.

*5.1.4. [BuTPP][FSI] (**4**).* Compound **4** was synthesized in the same manner as **1** using LiFSI as the anion source (0.23 g, 81% yield).

^{1}H NMR (400 MHz; $CDCl_3$) δ 7.82 (td, J = 7.4, 1.6 Hz, 3H), 7.74−7.62 (m, 12H), 3.16−3.08 (m, 2H), 1.64−1.55 (m, 4H), 0.92 (d, J = 13.9 Hz, 3H).

^{13}C NMR (101 MHz; $CDCl_3$) δ 135.4, 133.4, 130.7, 117.8, 24.4, 23.7, 22.3, 13.4.

^{19}F NMR (376 MHz; $CDCl_3$) δ −78.6.

■ ASSOCIATED CONTENT

Supporting Information

The Supporting Information is available free of charge at https://pubs.acs.org/doi/10.1021/acsomega.1c05241.

Crystallographic data for compound **1** (CIF)
Crystallographic data for compound **2** (CIF)
Crystallographic data for compound **3** (CIF)
Crystallographic data for compound **4** (CIF)
Percent interactions of the cations for compounds **1**−**4** as calculated from the Hirshfeld surfaces (Table S1); tabulated thermal data from all 3 cycles of DSC for the melting points T_m (Table S2); ^{1}H NMR for compound **1** (Figure S1); ^{13}C NMR for compound **1** (Figure S2); ^{19}F NMR for compound **1** (Figure S3); ^{1}H NMR for compound **2** (Figure S4); ^{13}C NMR for compound **2** (Figure S5); ^{19}F NMR for compound **2** (Figure S6); ^{1}H NMR for compound **3** (Figure S7); ^{13}C NMR for compound **3** (Figure S8); ^{19}F NMR for compound **3** (Figure S9); ^{1}H NMR for compound **4** (Figure S10); ^{13}C NMR for compound **4** (Figure S11); ^{19}F NMR for compound **4** (Figure S12); DSC traces for compound **1** (Figure S13); DSC traces for compound **2** (Figure S14); DSC traces for compound **3** (Figure S15); and DSC traces for compound **4** (Figure S16) (PDF)

■ AUTHOR INFORMATION

Corresponding Authors

Arsalan Mirjafari − *Department of Chemistry and Physics, Florida Gulf Coast University, Fort Myers, Florida 33965, United States;* orcid.org/0000-0002-5502-0602; Email: amirjafari@fgcu.edu

Patrick C. Hillesheim − *Department of Chemistry and Physics, Ave Maria University, Ave Maria, Florida 34142, United States; Department of Chemistry and Physics, Florida Gulf Coast University, Fort Myers, Florida 33965, United States;* orcid.org/0000-0002-9567-4002; Email: Patrick.Hillesheim@avemaria.edu

Authors

Brianna O'Rourke − *Department of Chemistry and Physics, Ave Maria University, Ave Maria, Florida 34142, United States*

Clare Lauderback − *Department of Chemistry and Physics, Ave Maria University, Ave Maria, Florida 34142, United States*

Lara I. Teodoro − *Department of Chemistry and Physics, Ave Maria University, Ave Maria, Florida 34142, United States*

Morgan Grimm − *Department of Chemistry and Physics, Ave Maria University, Ave Maria, Florida 34142, United States*

Matthias Zeller − *Department of Chemistry, Purdue University, West Lafayette, Indiana 47907, United States;* orcid.org/0000-0002-3305-852X

Gary L. Guillet − *Department of Chemistry and Biochemistry, Georgia Southern University, Savannah, Georgia 31419, United States;* orcid.org/0000-0002-3696-363X

Complete contact information is available at: https://pubs.acs.org/10.1021/acsomega.1c05241

Author Contributions

$^{\perp}$B.O., C.L., and L.I.T. contributed equally to this work.

Notes

The authors declare no competing financial interest.

■ ACKNOWLEDGMENTS

This work was supported by the Ave Maria University Department of Chemistry and Physics; part of this material is based upon work supported by the National Science Foundation through the Major Research Instrumentation Program under Grants Nos. CHE-1530959, CHE-1919785, and CHE-162554. A.M. would like to thank the National Science Foundation, RUI Program (CHE-1952846) for financial support.

■ REFERENCES

(1) MacFarlane, D. R.; Kar, M.; Pringle, J. M. *Fundamentals of Ionic Liquids*; Wiley-VCH Verlag GmbH & Co. KGaA: Weinheim, Germany, 2017.

(2) Welton, T. Ionic Liquids: A Brief History. *Biophys. Rev.* **2018**, *10*, 691−706.

(3) Fuller, J.; Carlin, R. T.; De Long, H. C.; Haworth, D. Structure of 1-Ethyl-3-Methylimidazolium Hexafluorophosphate: Model for Room Temperature Molten Salts. *J. Chem. Soc., Chem. Commun.* **1994**, No. 299.

(4) Wilkes, J. S.; Zaworotko, M. J. Air and Water Stable I-Ethyl-3-Methylimidazolium Based Ionic Liquids. *J. Chem. Soc., Chem. Commun.* **1992**, 965−967.

(5) Plechkova, N. V.; Seddon, K. R. *Ionic Liquids Completely UnCOILed: Critical Expert Overviews*; John Wiley & Sons, Inc.: Hoboken, NJ, 2015.

(6) Watanabe, M.; Thomas, M. L.; Zhang, S.; Ueno, K.; Yasuda, T.; Dokko, K. Application of Ionic Liquids to Energy Storage and Conversion Materials and Devices. *Chem. Rev.* **2017**, *117*, 7190−7239.

(7) Wang, B.; Qin, L.; Mu, T.; Xue, Z.; Gao, G. Are Ionic Liquids Chemically Stable? *Chem. Rev.* **2017**, *117*, 7113−7131.

(8) Fredlake, C. P.; Crosthwaite, J. M.; Hert, D. G.; Aki, S. N. V. K.; Brennecke, J. F. Thermophysical Properties of Imidazolium-Based Ionic Liquids. *J. Chem. Eng. Data* **2004**, *49*, 954−964.

(9) Crosthwaite, J. M.; Muldoon, M. J.; Dixon, J. K.; Anderson, J. L.; Brennecke, J. F. Phase Transition and Decomposition Temperatures, Heat Capacities and Viscosities of Pyridinium Ionic Liquids. *J. Chem. Thermodyn.* **2005**, *37*, 559−568.
(10) Zech, O.; Stoppa, A.; Buchner, R.; Kunz, W. The Conductivity of Imidazolium-Based Ionic Liquids from (248 to 468) K. B. Variation of the Anion †. *J. Chem. Eng. Data* **2010**, *55*, 1774−1778.
(11) Silva, W.; Zanatta, M.; Ferreira, A. S.; Corvo, M. C.; Cabrita, E. J. Revisiting Ionic Liquid Structure-Property Relationship: A Critical Analysis. *Int. J. Mol. Sci.* **2020**, *21*, No. 7745.
(12) Philippi, F.; Welton, T. Targeted Modifications in Ionic Liquids − from Understanding to Design. *Phys. Chem. Chem. Phys.* **2021**, *23*, 6993−7021.
(13) Dupont, J. On the Solid, Liquid and Solution Structural Organization of Imidazolium Ionic Liquids. *J. Braz. Chem. Soc.* **2004**, *15*, 341−350.
(14) Wang, Y.-L.; Li, B.; Sarman, S.; Mocci, F.; Lu, Z.-Y.; Yuan, J.; Laaksonen, A.; Fayer, M. D. Microstructural and Dynamical Heterogeneities in Ionic Liquids. *Chem. Rev.* **2020**, *120*, 5798−5877.
(15) Richter, K.; Dorn, K. V.; Smetana, V.; Mudring, A.-V. Elucidating Structure−Property Relationships in Imidazolium-Based Halide Ionic Liquids: Crystal Structures and Thermal Behavior. *Z. Kristallogr. - Cryst. Mater.* **2020**, *235*, 365−374.
(16) Atefi, F.; Garcia, M. T.; Singer, R. D.; Scammells, P. J. Phosphonium Ionic Liquids: Design, Synthesis and Evaluation of Biodegradability. *Green Chem.* **2009**, *11*, No. 1595.
(17) Fraser, K. J.; MacFarlane, D. R. Phosphonium-Based Ionic Liquids: An Overview. *Aust. J. Chem.* **2009**, *62*, No. 309.
(18) Holding, A. J.; Parviainen, A.; Kilpeläinen, I.; Soto, A.; King, A. W. T.; Rodríguez, H. Efficiency of Hydrophobic Phosphonium Ionic Liquids and DMSO as Recyclable Cellulose Dissolution and Regeneration Media. *RSC Adv.* **2017**, *7*, 17451−17461.
(19) Sowmiah, S.; Srinivasadesikan, V.; Tseng, M.-C.; Chu, Y.-H. On the Chemical Stabilities of Ionic Liquids. *Molecules* **2009**, *14*, 3780−3813.
(20) Ferreira, A. F.; Simões, P. N.; Ferreira, A. G. M. Quaternary Phosphonium-Based Ionic Liquids: Thermal Stability and Heat Capacity of the Liquid Phase. *J. Chem. Thermodyn.* **2012**, *45*, 16−27.
(21) Oh, S.; Morales-Collazo, O.; Keller, A. N.; Brennecke, J. F. Cation−Anion and Anion−CO 2 Interactions in Triethyl(Octyl)-Phosphonium Ionic Liquids with Aprotic Heterocyclic Anions (AHAs). *J. Phys. Chem. B* **2020**, 8877−8887.
(22) Skoronski, E.; Fernandes, M.; Malaret, F. J.; Hallett, J. P. Use of Phosphonium Ionic Liquids for Highly Efficient Extraction of Phenolic Compounds from Water. *Sep. Purif. Technol.* **2020**, *248*, No. 117069.
(23) Zielonka, J.; Joseph, J.; Sikora, A.; Hardy, M.; Ouari, O.; Vasquez-Vivar, J.; Cheng, G.; Lopez, M.; Kalyanaraman, B. Mitochondria-Targeted Triphenylphosphonium-Based Compounds: Syntheses, Mechanisms of Action, and Therapeutic and Diagnostic Applications. *Chem. Rev.* **2017**, *117*, 10043−10120.
(24) Parshall, G. W.; Shive, L. W.; Cotton, F. A. Phosphine Complexes of Rhenium. In *Inorganic Syntheses*; MacDiarmid, A. G., Ed.; John Wiley & Sons, Inc.: Hoboken, NJ, 2007; pp 110−112.
(25) Manzer, L. E.; Parshall, G. W. Lewis Acid Adducts of Trans-Hydrocyanobis(Triethylphosphine)Platinum. *Inorg. Chem.* **1976**, *15*, 3114−3116.
(26) Knifton, J. F. Ethylene Glycol from Synthesis Gas via Ruthenium Melt Catalysis. *J. Am. Chem. Soc.* **1981**, *103*, 3959−3961.
(27) Knifton, J. F. Vicinal Glycol Esters from Synthesis Gas. *J. Chem. Soc., Chem. Commun.* **1981**, No. 188.
(28) Knifton, J. F.; Grigsby, R. A.; Lin, J. J. Syngas Reactions. 6. Aliphatic Alcohols and Esters from Synthesis Gas. *Organometallics* **1984**, *3*, 62−69.
(29) Bradaric, C. J.; Downard, A.; Kennedy, C.; Robertson, A. J.; Zhou, Y. Industrial Preparation of Phosphonium Ionic Liquids. In *Ionic Liquids as Green Solvents*; Rogers, R. D.; Seddon, K. R., Eds.; ACS Symposium Series; American Chemical Society: Washington, DC, 2003; Vol. *856*, pp 41−56.
(30) Winterton, N. Crystallography of Ionic Liquids. In *Ionic Liquids Completely UnCOILed*; John Wiley & Sons, Ltd., 2015; pp 231−534.
(31) Teodoro, L. I.; Bellia, S. A.; Zeller, M.; Hillesheim, P. C. Examining the Interactions of a Thermally Robust Task-Specific Phosphonium-Based Ionic Compound. *Chem. Data Collect.* **2021**, *35*, No. 100760.
(32) McKinnon, J. J.; Mitchell, A. S.; Spackman, M. A. Hirshfeld Surfaces: A New Tool for Visualising and Exploring Molecular Crystals. *Chem. - Eur. J.* **1998**, *4*, 2136−2141.
(33) Spackman, M. A.; McKinnon, J. J. Fingerprinting Intermolecular Interactions in Molecular Crystals. *CrystEngComm* **2002**, *4*, 378−392.
(34) Spackman, M. A.; Jayatilaka, D. Hirshfeld Surface Analysis. *CrystEngComm* **2009**, *11*, 19−32.
(35) McKinnon, J. J.; Fabbiani, F. P. A.; Spackman, M. A. Comparison of Polymorphic Molecular Crystal Structures through Hirshfeld Surface Analysis. *Cryst. Growth Des.* **2007**, *7*, 755−769.
(36) Sun, J.; Wang, L.; Zhang, S.; Li, Z.; Zhang, X.; Dai, W.; Mori, R. ZnCl2/Phosphonium Halide: An Efficient Lewis Acid/Base Catalyst for the Synthesis of Cyclic Carbonate. *J. Mol. Catal. A: Chem.* **2006**, *256*, 295−300.
(37) *CrysAlisPRO, Oxford Diffraction/Agilent Technologies UK Ltd, Yarnton, England*; Oxford Diffraction/Agilent Technologies UK Ltd.: Yarnton, England.
(38) *Apex3 V2019.1-0, SAINT V8.40A*; Bruker AXS Inc.: Madison, WI, 2019.
(39) Krause, L.; Herbst-Irmer, R.; Sheldrick, G. M.; Stalke, D. Comparison of Silver and Molybdenum Microfocus X-Ray Sources for Single-Crystal Structure Determination. *J. Appl. Crystallogr.* **2015**, *48*, 3−10.
(40) *SHELXTL Suite of Programs, Version 6.14, 2000-2003, Bruker Advanced X-Ray Solutions*; Bruker AXS Inc.: Madison, WI.
(41) Sheldrick, G. M. A Short History of SHELX. *Acta Crystallogr., Sect. A: Found. Crystallogr.* **2008**, *64*, 112−122.
(42) Sheldrick, G. M. SHELXT − Integrated Space-Group and Crystal-Structure Determination. *Acta Crystallogr., Sect. A: Found. Adv.* **2015**, *71*, 3−8.
(43) Sheldrick, G. M. Crystal Structure Refinement with SHELXL. *Acta Crystallogr., Sect. C: Struct. Chem.* **2015**, *71*, 3−8.
(44) Hübschle, C. B.; Sheldrick, G. M.; Dittrich, B. ShelXle: A Qt Graphical User Interface for SHELXL. *J. Appl. Crystallogr.* **2011**, *44*, 1281−1284.
(45) Dolomanov, O. V.; Bourhis, L. J.; Gildea, R. J.; Howard, J. A. K.; Puschmann, H. OLEX2: A Complete Structure Solution, Refinement and Analysis Program. *J. Appl. Crystallogr.* **2009**, *42*, 339−341.
(46) Turner, M. J.; McKinnon, J. J.; Wolff, S. K.; Grimwood, D. J.; Spackman, P. R.; Jayatilaka, D.; Spackman, M. A. *CrystalExplorer17*; University of Western Australia, 2017.
(47) Spackman, P. R.; Turner, M. J.; McKinnon, J. J.; Wolff, S. K.; Grimwood, D. J.; Jayatilaka, D.; Spackman, M. A. CrystalExplorer: A Program for Hirshfeld Surface Analysis, Visualization and Quantitative Analysis of Molecular Crystals. *J. Appl. Crystallogr.* **2021**, *54*, 1006−1011.
(48) Mardirossian, N.; Head-Gordon, M. ΩB97X-V: A 10-Parameter, Range-Separated Hybrid, Generalized Gradient Approximation Density Functional with Nonlocal Correlation, Designed by a Survival-of-the-Fittest Strategy. *Phys. Chem. Chem. Phys.* **2014**, *16*, 9904.
(49) Groom, C. R.; Allen, F. H. The Cambridge Structural Database in Retrospect and Prospect. *Angew. Chem., Int. Ed.* **2014**, *53*, 662−671.
(50) Rocha, M. A. A.; Neves, C. M. S. S.; Freire, M. G.; Russina, O.; Triolo, A.; Coutinho, J. A. P.; Santos, L. M. N. B. F. Alkylimidazolium Based Ionic Liquids: Impact of Cation Symmetry on Their Nanoscale Structural Organization. *J. Phys. Chem. B* **2013**, *117*, 10889−10897.
(51) Burgess, K. M. N.; Korobkov, I.; Bryce, D. L. A Combined Solid-State NMR and X-Ray Crystallography Study of the Bromide

Ion Environments in Triphenylphosphonium Bromides. *Chem. - Eur. J.* **2012**, *18*, 5748−5758.
(52) Czerwinski, E. W. Butyltriphenylphosphonium Bromide. *Acta Crystallogr., Sect. E: Struct. Rep. Online* **2005**, *61*, o2272−o2273.
(53) Sharutin, V. V.; Egorova, I. V.; Klepikov, N. N.; Boyarkina, E. A.; Sharutina, O. K. Bismuth Compounds [Ph3BuP]+I−, [Ph3BuP] 2 + [Bi2I8 · 2Me2C=O]2−, and [Ph3BuP] 2 + [Bi2I8 · 2Me2S=O]2−: Syntheses and Crystal Structures. *Russ. J. Coord. Chem.* **2009**, *35*, 186−190.
(54) Reichert, W. M.; Holbrey, J. D.; Swatloski, R. P.; Gutowski, K. E.; Visser, A. E.; Nieuwenhuyzen, M.; Seddon, K. R.; Rogers, R. D. Solid-State Analysis of Low-Melting 1,3-Dialkylimidazolium Hexafluorophosphate Salts (Ionic Liquids) by Combined X-Ray Crystallographic and Computational Analyses. *Cryst. Growth Des.* **2007**, *7*, 1106−1114.
(55) Dean, P. M.; Pringle, J. M.; Forsyth, C. M.; Scott, J. L.; MacFarlane, D. R. Interactions in Bisamide Ionic Liquids—Insights from a Hirshfeld Surface Analysis of Their Crystalline States. *New J. Chem.* **2008**, *32*, 2121.
(56) Preiss, U. P.; Zaitsau, D. H.; Beichel, W.; Himmel, D.; Higelin, A.; Merz, K.; Caesar, N.; Verevkin, S. P. Estimation of Lattice Enthalpies of Ionic Liquids Supported by Hirshfeld Analysis. *ChemPhysChem* **2015**, *16*, 2890−2898.
(57) Gouveia, A. S. L.; Bernardes, C. E. S.; Tomé, L. C.; Lozinskaya, E. I.; Vygodskii, Y. S.; Shaplov, A. S.; Lopes, J. N. C.; Marrucho, I. M. Ionic Liquids with Anions Based on Fluorosulfonyl Derivatives: From Asymmetrical Substitutions to a Consistent Force Field Model. *Phys. Chem. Chem. Phys.* **2017**, *19*, 29617−29624.
(58) Siu, B.; Cassity, C. G.; Benchea, A.; Hamby, T.; Hendrich, J.; Strickland, K. J.; Wierzbicki, A.; Sykora, R. E.; Salter, E. A.; O'Brien, R. A.; West, K. N.; Davis, J. H. Thermally Robust: Triarylsulfonium Ionic Liquids Stable in Air for 90 Days at 300 °C. *RSC Adv.* **2017**, *7*, 7623−7630.
(59) Zhao, M.; Wu, B.; Lall-Ramnarine, S. I.; Ramdihal, J. D.; Papacostas, K. A.; Fernandez, E. D.; Sumner, R. A.; Margulis, C. J.; Wishart, J. F.; Castner, E. W. Structural Analysis of Ionic Liquids with Symmetric and Asymmetric Fluorinated Anions. *J. Chem. Phys.* **2019**, *151*, No. 074504.
(60) Traver, J.; Chenard, E.; Zeller, M.; Guillet, G. L.; Lynch, W. E.; Hillesheim, P. C. Directing Cation-Cation Interactions in Thiamine Compounds: Analysis of a Series of Organic Salts Based on Vitamin B1. *J. Mol. Struct.* **2021**, *1232*, No. 130046.
(61) Fujii, K.; Seki, S.; Fukuda, S.; Kanzaki, R.; Takamuku, T.; Umebayashi, Y.; Ishiguro, S. Anion Conformation of Low-Viscosity Room-Temperature Ionic Liquid 1-Ethyl-3-Methylimidazolium Bis-(Fluorosulfonyl) Imide. *J. Phys. Chem. B* **2007**, *111*, 12829−12833.
(62) Malathy Sony, S. M.; Ponnuswamy, M. N. Nature of π-Interactions in Nitrogen-Containing Heterocyclic Systems: A Structural Database Analysis. *Cryst. Growth Des.* **2006**, *6*, 736−742.
(63) Kamavaram, V.; Reddy, R. G. Thermal Stabilities of Di-Alkylimidazolium Chloride Ionic Liquids. *Int. J. Therm. Sci.* **2008**, *47*, 773−777.
(64) Rabideau, B. D.; West, K. N.; Davis, J. H. Making Good on a Promise: Ionic Liquids with Genuinely High Degrees of Thermal Stability. *Chem. Commun.* **2018**, *54*, 5019−5031.
(65) Serra, P. B. P.; Ribeiro, F. M. S.; Rocha, M. A. A.; Fulem, M.; Růžička, K.; Santos, L. M. N. B. F. Phase Behavior and Heat Capacities of the 1-Benzyl-3-Methylimidazolium Ionic Liquids. *J. Chem. Thermodyn.* **2016**, *100*, 124−130.
(66) *Structures and Interactions of Ionic Liquids*; Zhang, S.; Wang, J.; Lu, X.; Zhou, Q., Eds.; Structure and Bonding; Springer Berlin Heidelberg: Berlin, Heidelberg, 2014; Vol. *151*.
(67) Holbrey, J. D.; Reichert, W. M.; Rogers, R. D. Crystal Structures of Imidazolium Bis(Trifluoromethanesulfonyl)Imide 'Ionic Liquid' Salts: The First Organic Salt with a Cis-TFSI Anion Conformation. *Dalton Trans.* **2004**, 2267−2271.
(68) Langevin, D.; Nguyen, Q. T.; Marais, S.; Karademir, S.; Sanchez, J.-Y.; Iojoiu, C.; Martinez, M.; Mercier, R.; Judeinstein, P.; Chappey, C. High-Temperature Ionic-Conducting Material: Advanced Structure and Improved Performance. *J. Phys. Chem. C* **2013**, *117*, 15552−15561.
(69) Welton, T. Room-Temperature Ionic Liquids. Solvents for Synthesis and Catalysis. *Chem. Rev.* **1999**, *99*, 2071−2084.
(70) Saouane, S.; Norman, S. E.; Hardacre, C.; Fabbiani, F. P. A. Pinning down the Solid-State Polymorphism of the Ionic Liquid [Bmim][PF6]. *Chem. Sci.* **2013**, *4*, No. 1270.
(71) Heravi, M. M.; Ghanbarian, M.; Zadsirjan, V.; Alimadadi Jani, B. Recent Advances in the Applications of Wittig Reaction in the Total Synthesis of Natural Products Containing Lactone, Pyrone, and Lactam as a Scaffold. *Monatsh. Chem. - Chem. Mon.* **2019**, *150*, 1365−1407.
(72) Knouse, K. W.; Flood, D. T.; Vantourout, J. C.; Schmidt, M. A.; Mcdonald, I. M.; Eastgate, M. D.; Baran, P. S. Nature Chose Phosphates and Chemists Should Too: How Emerging P(V) Methods Can Augment Existing Strategies. *ACS Cent. Sci.* **2021**, *7*, 1473−1485.

https://doi.org/10.1021/acsomega.1c05241
ACS Omega 2021, 6, 32285−32296